*R*esearch in
*A*stronomy and
*A*strophysics

Space weathering of the Moon from *in situ* detection⋆

Yun-Zhao Wu[1,2,3], Zhen-Chao Wang[4] and Yu Lu[5,6]

[1] Key Laboratory of Planetary Sciences, Purple Mountain Observatory, Chinese Academy of Sciences, Nanjing 210034, China; *wu@pmo.ac.cn*
[2] Space Science Institute, Macau University of Science and Technology, Macau, China
[3] CAS Center for Excellence in Comparative Planetology, China
[4] Institute of Surficial Geochemistry, Department of Earth Sciences, Nanjing University, Nanjing 210023, China
[5] School of Geographic and Oceanographic Sciences, Nanjing University, Nanjing 210023, China
[6] Jiangsu Center for Collaborative Innovation in Geographical Information Resource Development and Application, Nanjing 210023, China

Abstract Space weathering is an important surface process that occurs on the Moon and other airless bodies, especially those that have no magnetic field. The optical effects of the Moon's space weathering have largely been investigated in the laboratory for lunar samples and lunar analogues. However, duplication of pristine regolith on Earth is not possible. Here we report on space weathering from the unique perspective of the "*Yutu*" rover, which was part of the *Chang'e-3* (*CE-3*) mission, building on our previous work. Measurement of the visually undisturbed uppermost regolith as well as locations that have been affected by rocket exhaust from the spacecraft by the Visible-Near Infrared Spectrometer (VNIS) revealed that the returned samples provide biased information about the pristine lunar regolith. The uppermost surficial regolith is much more weathered than the regolith immediately below, and the finest fraction is rich in space weathered products. These materials are very dark and attenuated throughout the visible and near-infrared (VNIR) wavelengths, hence reducing the reflectance and masking the absorption features. The effects on the spectral slope caused by space weathering are wavelength-dependent: the visible and near-infrared continuum slope (VNCS) increases while the visible slope (VS) decreases. In the visible wavelengths, the optical effects of space weathering and TiO_2 are identical: both reduce albedo and blue the spectra. This suggests that a new TiO_2 abundance algorithm is needed. Optical maturity indices are related to composition and hence only locally meaningful. Since optical remote sensing can only sense the uppermost few microns of regolith and since this surface tends to be very weathered, the interpretation of surface composition using optical remote sensing data needs to be carefully evaluated. Sampling the uppermost surface is suggested.

Key words: Moon — evolution — spectroscopic — data analysis

1 INTRODUCTION

Space weathering is a continuous and primary surface process occurring on the Moon and other airless bodies, especially those that are not protected by a magnetic field. This process is caused by various external forces, including agglutination and disaggregation by meteoroid impacts, implantation of ions from the solar wind, and sputtering by solar and Galactic ions and high energy photons. All of these processes cause the regolith to mature, the degree to which is described as maturity. The products of space weathering are agglutinitic glasses, submicroscopic iron (SMFe), amorphous coatings on grains, new minerals and accumulation of meteoritic materials (e.g., Morris 1976; Keller & McKay 1997; Anand et al. 2004). The specific ferromagnetic resonance intensity normalized to the total iron content (Is/FeO) suggested by Cirlin et al. (1974), Housley et al. (1975), Pearce et al. (1974) and Morris (1976) is the standard measure of regolith maturity based

upon the reduction of FeO to metallic Fe. Other indices of maturity include abundance of agglutinates, concentration of solar-wind-implanted gases and particle size (Jolliff et al. 2006). All these indices of maturity were derived from the investigation of bulk soils.

Space weathering is of considerable interest because it causes changes in the optical properties of surfaces. On the Moon, it reduces the visible and near-infrared (VNIR) albedo and the strength of absorption bands (band depth and band area), and increases spectral slope (Hapke 2001; Lucey et al. 2006; Pieters & Noble 2016). Based on these optical effects, several optical maturity indices have been created to investigate the relative age of craters, physical processes on the lunar surface, and the reduction of elements and minerals. Among these, the optical maturity parameter (OMAT) proposed by Lucey et al. (2000) is the most commonly used for remote mapping of maturity on the lunar surface. It is the Euclidean distance from hypothetically fully matured (dark red) origin to the point of interest in a scatterplot of 750 nm reflectance versus 950/750 nm reflectance ratio. Other optical maturity indices are near-infrared (NIR)/visible (VIS) ratio (e.g., Fischer & Pieters 1996) and normalized visible and near-infrared continuum slope (VNCS-N) (e.g., Fischer & Pieters 1994; Hiroi et al. 1997; Le Mouélic et al. 2000).

Understanding the effects of space weathering on reflectance spectra is crucial for the interpretation of elements and minerals using remote sensing data. Numerous experimental approaches on lunar samples (Keller & McKay 1993; Noble et al. 2001; Keller et al. 2016) and analogs (Noble et al. 2007) have been performed to investigate space weathering. However, none of these can realistically duplicate the actual conditions on the lunar surface. The *in situ* spectra measured by the Visible-Near Infrared Spectrometer (VNIS) onboard the "*Yutu*" rover, which was part of the *Chang'e-3* (*CE-3*) mission, provide a unique opportunity for investigating space weathering by measuring the regolith in its undisturbed state, as well as comparing with the regolith naturally disturbed by rocket exhaust from the spacecraft. For example, using the *CE-3 in situ* spectra, Wang et al. (2017) estimated the SMFe abundance of the *CE-3* landing site to be 0.368 wt.% by means of Hapke's model. In this paper, we report on further analysis of space weathering as measured by the *CE-3 in situ* spectra.

2 DATA AND METHODS

2.1 Instrument and Data

The VNIS consists of a VIS/NIR imaging spectrometer (450–950 nm), a shortwave infrared (SWIR) spectrometer

(900–2395 nm) and a white calibration panel. There are 100 channels for the VIS spectrometer and 300 channels for the SWIR spectrometer with the same spectral sampling interval of 5 nm. *CE-3* landed on the rim of Zi Wei crater which is in northern Mare Imbrium. The landing site belongs to the unsampled, spectrally unique late-stage basalts according to their relatively strong 1000 nm feature and weaker 2000 nm absorption compared with older basalts (Staid et al. 2011; Wu et al. 2018a). These young basalts have high scientific significance because they provide key information on the late-stage evolution of the Moon. Four measurements (sites 5, 6, 7 and 8) of the soil were made by the VNIS during the period that *Yutu* was mobile. The locations of the four measurements are shown in Figure 1. Details of the instrument, data processing and calibration are provided in Wu & Hapke (2018) and Wu et al. (2018b).

During the two lunar-day measurements by the VNIS between 2013 December 23 and 2014 January 14, the farthest target measured was about 40 m from the lander and only regoliths with no rocks were measured. For comparison, data from the Moon Mineralogy Mapper (M³) (*https://pds-imaging.jpl.nasa.gov/data/m3/*), which was aboard the Indian mission *Chandrayaan-1*, were also used in this study. M³ is a hyperspectral instrument with 85 bands in its global mode. In this paper, we used the Level 2 (L2) reflectance products acquired during the Optical Period 1B (OP1B), which have the highest spatial resolution (140 m/p). The L2 data have been photometrically corrected to standard geometry (30°, 0°, 30°) and corrected for thermal emissions. Three M³ spectra from the landing site, Zi Wei crater, and a 350 m very fresh crater located 4.7 km southwest of the *CE-3* landing site (see fig. 1b in Wu & Hapke (2018) for detailed location) were extracted. They represented three mature states from soils to rocks.

2.2 Spectral Parameter Analysis

Several spectral parameters including band center (BC), band depth (BD), band area (BA), visible and near-infrared continuum slope (VNCS), visible slope (VS), band ratio (BR) and OMAT were calculated. The VNCS is defined as the slope of a line covering the 1000 nm absorption that connects two local spectral maxima of its two sides. It was calculated for two types of data and given two names for convenience: 1) the original reflectance (named VNCS), and 2) the reflectance normalized at 750 nm (named VNCS-N). The latter is similar to the continuum slope used previously (Fischer & Pieters 1994; Hiroi et al. 1997; Le Mouélic et al. 2000), which
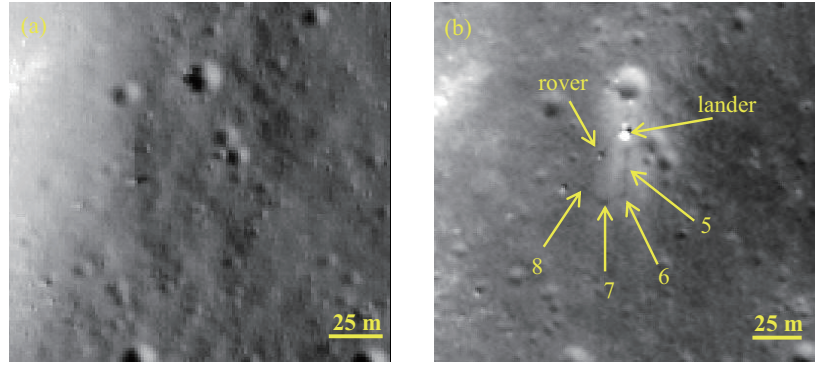
Fig. 1 The Lunar Reconnaissance Orbiter Camera (LROC) Narrow Angle Camera (NAC) images of the *CE-3* landing site. (a) before landing (NAC image M1127248516R). (b) after landing (NAC image M1147290066R).
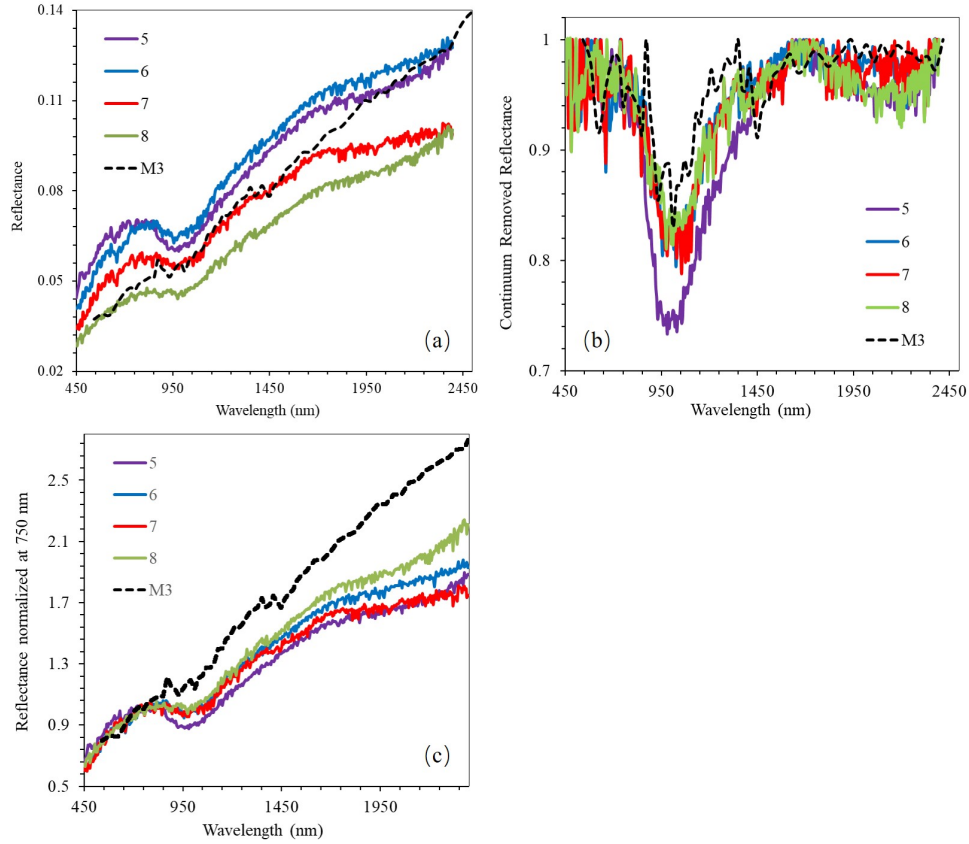

Fig. 2 (a) The VNIS reflectance spectra, (b) the continuum removed spectra and (c) reflectance spectra normalized at 750 nm for four sites. Also shown are M^3 spectra of regolith.

is defined as the slope of a straight line fit tangent to both sides of the 1000 nm band and then scaled to the short-wavelength point of tangency. The BR is 450/620 nm for VNIS (the VS will decrease at wavelengths longer than 620 nm) and 540/750 nm for M^3 (the shortest band of M^3 is 540 nm). The OMAT was calculated using the formula in Lucey et al. (2000). Before the spectral calculation, all the VNIS and M^3 spectra were smoothed by B-spline fitting.

To calculate BC, BD, BA and VNCS, it is necessary to derive the spectral continuum. In this study, the straight-

line continuum was used. The spectral subset (i.e., the two endpoints) for the automatic algorithm deriving the two tangents was assigned using the method developed in Wu et al. (2018a) because the reflectance continuously increases in the infrared bands due to thermal emission from the lunar surface. The BC was calculated by fitting a 6th order polynomial to the bottom quarter of the continuum-removed absorption feature, and the minimum point on the polynomial fit is considered as the BC. The BD was calculated as follows: $D = 1 - R_b/R_c$, where R_b is the re-

flectance at the BC and R_c is the reflectance of the continuum at the same wavelength as R_b. The BA was defined as the area of the 1000 nm absorption feature for the continuum removed spectra. The spectral slope (both VNCS and VS) was calculated as follows: $\Delta\text{reflectance}/\Delta\lambda = (R_2 - R_1)/(\lambda_2 - \lambda_1)$, where R is reflectance and λ is wavelength. For the VNCS, λ_2 and λ_1 are the wavelengths of the two tangents covering the 1000 nm absorption. For the VS (named VS1), λ_2 and λ_1 are 620 and 450 nm for VNIS and 750 and 540 nm for M^3 respectively. Moreover, to avoid noise in representing slope with only two endpoints, the VS was also calculated using a linear fitting between 450 and 620 nm for VNIS and 540 and 730 nm for M^3. Similar to VNCS, it was also calculated for two types of data: (1) the original reflectance (named VS2), and (2) the reflectance normalized at the starting wavelength (named VS-N).

3 RESULTS

The four *in situ* reflectance spectra are displayed in Figure 2 and spectral parameters are listed in Table 1. The *in situ* spectra from all four sites exhibit characteristics of lunar soil in terms of increasing reflectance with increasing infrared wavelength and two absorptions near 1000 and 2000 nm, where the 1000 nm absorption is relatively strong and the 2000 nm absorption is very weak. The VNCS of the four measurements is similar. The VNCS-N, BR and BC approximately decrease for sites closer to the lander. The reflectance, absorption strength (BD and BA), VS and OMAT (OMAT increases with increasing immaturity) all increase for sites closer to the lander. The variations of these spectral parameters for *CE-3 in situ* spectra are consistent with those of M^3 data from regolith to fresh crater.

These variations of *in situ* spectra between different sites indicate that the maturity of regolith becomes less for sites closer to the lander. We propose that this happens because rocket exhaust blew away the uppermost mature dust and soils and exposed less-mature materials. Considering that the disturbance depth was very shallow and only the finest fraction of the regolith was disturbed, this suggests a different model of space weathering from that derived from lunar samples. The space weathering model from the lunar samples shows that (1) the finest fraction of lunar soils is enriched in Al_2O_3 and depleted in FeO and the brightest among all fractions of lunar soils (Pieters et al. 1993; Taylor et al. 2001), (2) maturity does not change significantly within the first tens of centimeters of regolith depth (Clegg et al. 2014) and (3) there appears to be little difference in soil properties inside and outside the blast zones (Clegg et al. 2014).
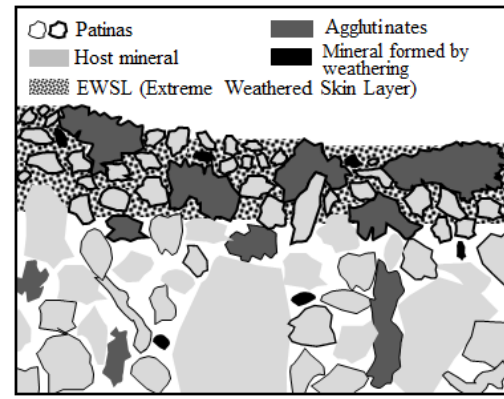

Fig. 3 Model for space weathering on the real lunar surface.

Figure 3 shows the enhanced space weathering model of the lunar surface based on *CE-3* observations:

(1) The uppermost surficial regolith, perhaps several millimeters to tens of centimeters thick, is much more weathered than the regolith immediately below (named the Extreme Weathered Skin Layer in this paper), and

(2) The finest fraction is much more mature than the coarser fraction. The weathered products are very dark and exhibit attenuated spectral features at all wavelengths, which mask the absorption features and reduce the overall reflectance of covered original minerals.

The remaining materials at Site 5, that is, material not removed by the lander rocket, have clear mafic absorptions, yet still these spectral features are attenuated relative to fresh mineral spectra. Site 5's *in situ* spectra also have a red VNCS. It is clear that Site 5 material contains a significant amount of space weathered products. The BD and OMAT values of Site 5 are similar to those of the fresh crater, and larger than those of the wall of Zi Wei crater derived from M^3 data. The wall of Zi Wei, which has numerous rocks, shows a similar BD but a little smaller BA and OMAT value compared to Site 6. Site 8 soil has a larger BD, BA and OMAT value than M^3 soil spectra of the landing site. These comparisons suggest that the *in situ* spectra are relatively optically immature compared to the orbital data (i.e., the lithic fragments/mineral fraction in the pixels of *in situ* spectra is more than that of the M^3 pixels). Further research is needed to resolve this issue.

4 DISCUSSION

4.1 Unrepresentativeness of Lunar Samples for Real Lunar Surface

Figure 1 shows that the brightness of the *CE-3* landing site increased after the spacecraft landed. The increase in the reflectance of the disturbed regolith was found for all the landing sites (Clegg et al. 2014). Smoothing of sur-

Table 1 Spectral parameters and optical maturity values of the VNIS and M^3 data. The unit for all spectral slopes is μm^{-1} and for BC it is nm.

	Site	BC	BR	BD	BA	OMAT	VNCS	VNCS-N	VS1	VS2	VS-N
VNIS	5	995.36	0.67	0.24	66.24	0.34	0.032	0.46	0.13	0.11	2.54
	6	1013.50	0.68	0.17	44.87	0.24	0.043	0.64	0.11	0.12	3.00
	7	1025.03	0.67	0.16	43.40	0.26	0.034	0.60	0.10	0.11	3.12
	8	1020.22	0.72	0.15	39.91	0.18	0.033	0.74	0.07	0.06	2.25
M^3	fresh crater	994.53	0.76	0.25	70.98	0.36	0.014	0.23	0.07	0.08	1.73
	Zi Wei	987.13	0.74	0.17	38.85	0.21	0.035	0.68	0.06	0.06	1.67
	regolith	1010.60	0.78	0.12	28.67	0.07	0.052	1.08	0.05	0.05	1.49

face roughness has been suggested as the main cause of the observed increase in reflectance after a spacecraft had landed (Kaydash et al. 2011; Shkuratov et al. 2013; Clegg et al. 2014). Exposure of less mature soil was rejected in these studies based on: (1) the Apollo core samples indicating that maturity does not change significantly within the first tens of centimeters of regolith depth, and (2) samples obtained using surface scoops appear to have little difference inside and outside the blast zones at the Apollo landing sites. The finding by VNIS that the maturity decreases immediately below the surface is contrary to lunar sample data. Another difference is the finest fraction. Almost all the sample spectra show that the $<10\,\mu m$ fractions are the brightest among all size fractions (Pieters et al. 1993). Sample analyses also demonstrate that for the finest fraction of the lunar soil ($<10\,\mu m$) the abundance of plagioclase mineral fragments increases, and is depleted in FeO and enriched in Al_2O_3 relative to bulk lunar soil (Pieters et al. 1993; Taylor et al. 2001), which would increase the albedo. However, as shown above, the finest fractions that were blown away are very dark and attenuated for a whole wavelength, though these finest fractions which were blown away include not only $<10\,\mu m$ fractions but also large particles. These findings indicate that the returned samples do not represent the uppermost and most weathered layer of lunar regolith. A visual comparison of terrestrial materials indicates that a desert varnish darkens rocks considerably.

4.2 Rapid Rate of SMFe Formation for the Skin Regolith

A recent study has found that the top two centimeters of regolith are churned very quickly, on a timescale of 81 000 years (Speyerer et al. 2016). The large difference between spectra of the skin regolith and immediately below derived from the *in situ* spectra indicates quick development of various space weathering products at the lunar surface compared to the vertical overturn. Wang et al. (2017) estimated that Site 8, the visually undisturbed soil, has 0.151 wt.%

SMFe higher than that of the mostly disturbed soil, Site 5. It suggests that continual bombardment of the regolith by solar wind, high energy cosmic rays and interplanetary dust particles results in a rapid development of SMFe and other space weathering products (e.g., agglutinates, mineral formed by weathering such as hapkeite (Anand et al. 2004), other submicroscopic metals, etc).

4.3 Reddening or Bluing?

The *in situ* spectra validate the lunar-style space weathering effects and yield new information. Canonical opinion believed that space weathering increases the spectral slope in the VIS and NIR (Lucey et al. 1998; Hapke 2001; Noble et al. 2001; Gillis et al. 2003), such that the 415/750 nm ratio of *Clementine* data becomes smaller with increasing maturity. The *in situ* spectra show the effects on the spectral slope caused by space weathering are wavelength-dependent: increasing the VNCS while decreasing the VS. Table 1 demonstrates that the VIS spectral slope gradually decreases from immature to mature soils, indicating that space weathering blues the surface rather than reddens it. This happens because SMFe and other space weathering products strongly absorb light throughout the VNIR wavelengths and hence reduce the spectral contrast (i.e., slope) between ultraviolet (UV) and VIS bands. In contrast, fresh materials and also bright materials exhibit a large spectral contrast in the VIS bands. This is caused by the strong charge-transfer absorptions due to the Fe^{2+} – Ti^{4+} or O-metal transitions in the UV extending to the VIS wavelengths. This finding that space weathering decreases the VS is consistent with UV observations of the Moon (Denevi et al. 2014) and asteroids (Hendrix & Vilas 2006), and extends to the VIS bands.

To validate the results from VNIS data, we further analyzed the VS using M^3, *Clementine* and LROC Wide Angle Camera (WAC) 7-channel mosaic data for the whole Moon. The analysis from all three global datasets shows that immature regolith exhibits a larger VS than more mature materials, consistent with the finding from the VNIS
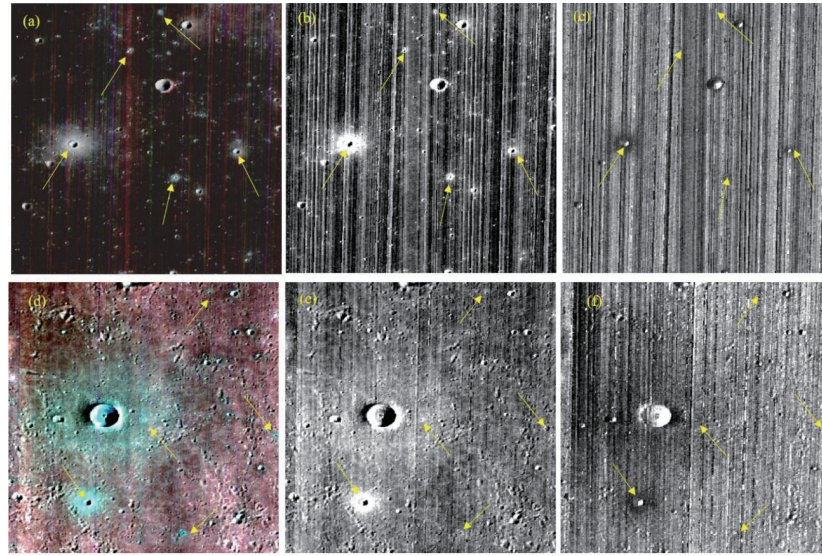
Fig. 4 M^3 images showing that space weathering reduces VIS spectral slope. (Fresh craters are marked with *arrows*.) *Top panel*: late-stage high-Fe basalts (similar to those at the *CE-3* landing site) with the location of the largest fresh crater at 40.085°N, −26.247°W. *Bottom panel*: old low-Ti basalts with the center of the image at 39.327°N, 0.119°E. (a) and (d) Color composite image (R-989 nm; G-750 nm; B-540 nm). (b) and (e) Difference image (730 nm–540 nm). (c) and (f) Ratio image (540 nm/730 nm). Note that fresh craters show a bright halo (larger slope) in the difference images (b and e) and dark halo (lower UV/VIS ratio) in the ratio images (c and f), indicating that fresh materials have larger VS than do mature materials.

data. In detail, bright halos in Figure 4(b) and (e) clearly indicate that the VS of relatively young craters is larger than surrounding regolith. Correspondingly, the 540/730 nm ratio of fresh craters is smaller than the surrounding regolith (e.g., dark halo in Fig. 4(c) and (f)). Our results are in contrast to previous results from *Clementine* data (Lucey et al. 1998; Gillis et al. 2003). Since the lunar TiO$_2$ abundance algorithm in Lucey et al. (1998) and Gillis et al. (2003) is based on the opinion that the UV/VIS ratio becomes smaller with increasing maturity, developing a new TiO$_2$ abundance algorithm is needed. Moreover, our results indicate much more complexity in the derivation of TiO$_2$ regolith abundances because the optical effects of TiO$_2$ and space weathering are identical, i.e., reducing albedo and bluing the regolith.

4.4 Indices of Maturity

The *in situ* spectra reveal a complex relationship between maturity indices (both chemical and optical) and space weathering. Previously, spectral researches on space weathering were focused mostly on VNCS and they concluded that the VNCS is directly correlated with the amount of Is. Good correlations between normalized VNCS (VNCS-N) and Is or Is/FeO have been reported in several papers (Fischer & Pieters 1994; Hiroi et al. 1997; Le Mouélic et al. 2000). These good correlations, however, could not be simply because VNCS of lunar soils is

caused by SMFe. The correlation observed by Fischer & Pieters (1994) is for maturity index Is/FeO while that observed by Hiroi et al. (1997) and Le Mouélic et al. (2000) is for Is (i.e., nanophase Fe) and there is no correlation with Is/FeO. The samples in Le Mouélic et al. (2000) show that the high FeO group has larger normalized VNCS and Is than the low FeO group. This just indicates that VNCS is caused by the inherent properties of the regolith (e.g., the FeO and TiO$_2$ abundances). For example, highlands have larger VNCS and VS than those of maria (fig. 6 in Wu et al. (2013) and table 1 in Le Mouélic et al. (2000)). For more detailed information see Figure 5, which demonstrates that VNCS and VS are negatively correlated with FeO. The continuum slope in these studies (Fischer & Pieters 1994; Hiroi et al. 1997; Le Mouélic et al. 2000) is not VNCS but VNCS-N. The performance of scaling or normalization to some band has the same influence on optical effects as space weathering because the low reflectance causes a much larger slope than a high reflectance.

Figure 5 shows that the normalized slopes (VNCS-N and VS-N) changed the negative correlation between FeO and slope. Table 1 and Figure 2(c) also indicate that the VNCS of Site 8 is almost the lowest while the VNCS-N of Site 8 becomes the largest because the reflectance of Site 8 is the lowest. This resolves the discrepancy found (1) in Denevi et al. (2014) that spectral trends related to space weathering are different for highlands and maria, and (2) the 415/750 ratio image featuring bright rays on the
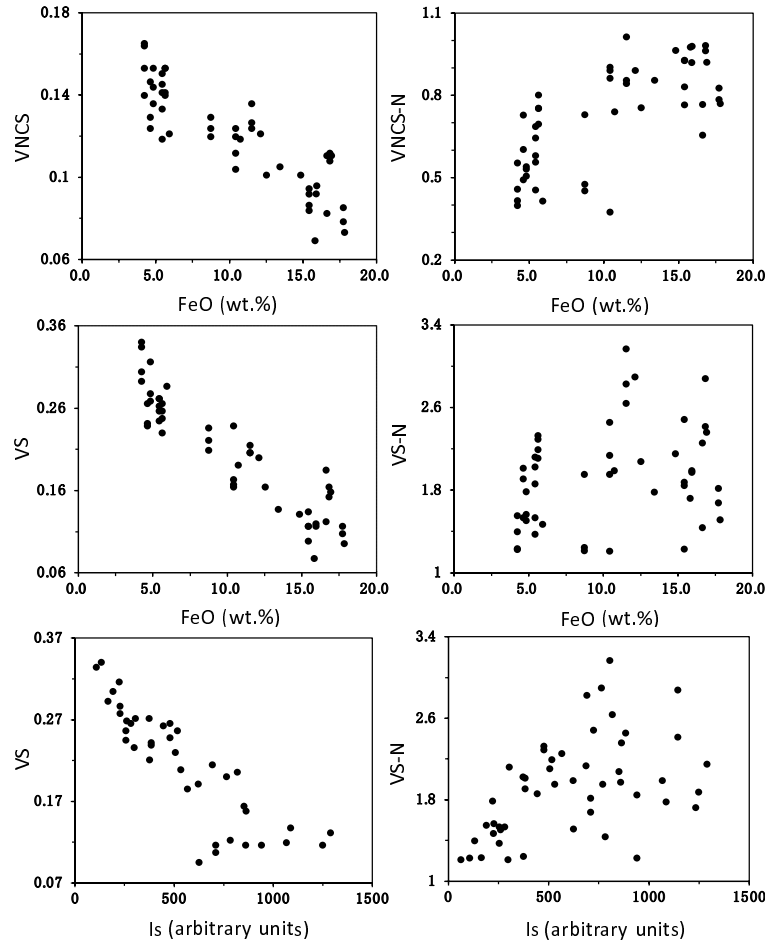
Fig. 5 Scatterplots of spectral parameters and chemical compositions in lunar soils. The data are from table 1 in Le Mouélic et al. (2000).

highlands (Fig. 6(d)) and bright halos surrounding fresh craters in some areas.

To confirm the VNIS results, we performed further analysis using M^3, *Clementine* and LROC WAC data of nearly the whole Moon. For each dataset, both the ratio image (reflectance of short wavelength divided by that of long wavelength) and the difference image (reflectance of long wavelength minus that of short wavelength) were calculated.

Figure 6 shows the results. The three datasets indicate that space weathering consistently reduces VS rather than increasing it. (Note that the difference of two bands represents the spectral slope while the ratio of two bands does not represent the spectral slope but the spectral normalization.) Moreover, to avoid the noise of two individual bands, an alternative method of calculation of the spectral slope can be a linear fit using multiple bands. This gives the same results as the difference between two bands.

Figure 6(d) and Denevi et al. (2014) used the reflectance ratio rather than the difference between two

bands as a measure of the spectral slope. When viewed in terms of the difference between two bands (i.e., the mathematically true slope), the spectral trends related to space weathering are the same for highlands and maria, i.e., immature regolith has a larger VS than its mature counterpart.

Figure 7 provides more illustration. It shows that the difference (i.e., the VS) is positively correlated with albedo for both highlands and mare while counterpart correlations appear with the ratio corresponding to highlands and mare. It also illustrates that the optical effects of TiO$_2$ and space weathering are identical because Ti also darkens and blues lunar soils (e.g., Charette et al. 1974).

In addition to VNCS, OMAT has been found to correlate well with Is/FeO (Lucey et al. 2000). However, this index also could not be simply thought of as related to SMFe or maturity. First, like the correlation between VNCS and Is or Is/FeO mentioned above, this correlation is not reliable because some used Is (Le Mouélic et al. 2000) while some used Is/FeO (Lucey et al. 2000). The correlation plot between VNCS and OMAT (Fig. 4(b) in Le Mouélic
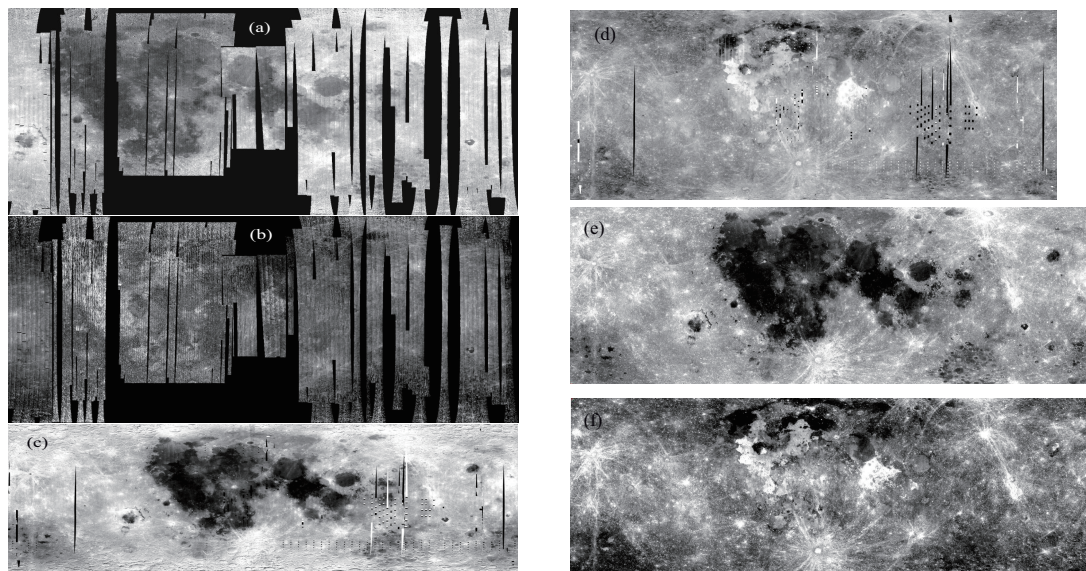
Fig. 6 Difference image (730–540 nm) (a) and ratio image (540 nm/730 nm) (b) of global M^3 data. (c) and (d), and (e) and (f) are similar to (a) and (b) but for *Clementine* (750 nm and 415 nm) and LROC WAC (689 nm and 415 nm) data respectively.

et al. 2000) shows that high TiO$_2$ samples have smaller OMAT values than low TiO$_2$ samples. This happens because OMAT is more affected by TiO$_2$ abundance than Is or Is/FeO in these data. TiO$_2$ reduces spectral contrast and albedo and so reduces OMAT, which is the same trend as the influence of space weathering. Therefore, using OMAT to represent maturity should be used with care, taking into account the Ti content of the surface regolith.

In summary, all the spectral parameters (e.g., brightness, VNCS, VS, BD, BA and OMAT) describe the optical effects of space weathering and can be used as optical maturity indices. All of them also describe the optical characteristics of compositions. The essence of the optical effects of space weathering is the compositional alteration. Therefore, whether for measuring maturity or evaluating composition, the spectral parameters are only valid locally. Previous researchers also note that OMAT works as a good measure of relative exposure age for a regional surface but not its absolute age because it is affected by several factors such as component and grain size (Le Mouélic et al. 2000; Lucey et al. 2000).

Figure 8(a) shows the plot of OMAT versus Is/FeO from the RELAB Lunar Soil Characterization Consortium (LSCC) (*http://www.planetary.brown.edu/pds/LSCCsoil.html*). Figure 8(b) displays the plot for high FeO samples with FeO >14 wt.%. As a whole, the correlation is not apparent. Only samples with high OMAT values display correlation and they correspond to immature soil. For low and middle FeO samples, the OMAT saturation with respect to Is/FeO is at 70. The maximum Is/FeO for high-FeO soils is <100, which

surprisingly is much lower than low and middle FeO soils. For high-FeO samples, the correlation is weakly consistent with the FeO and TiO$_2$ effects on OMAT, as discussed above. High TiO$_2$ soil samples and also bright materials (see Sect. 4.3 and 4.4 for a discussion of the spectral slope) exhibit lower OMAT values than low TiO$_2$ soils (Fig. 8b), supporting the above conclusion that TiO$_2$ has the same optical effects as space weathering and complicating the relationship between optical parameters and maturity. The age of the Zi Wei crater was estimated to be ∼100 Ma using its morphologic class (Basilevsky et al. 2015) or ∼120 Ma by comparing the crater morphology and rock abundances with Steno-Apollo crater (110 Ma) (Arvidson et al. 1976) and Camelot crater (143 Ma) (Drozd et al. 1977). These analyses indicate that the *CE-3* landing area is geologically young. The OMAT of *CE-3* soil, which has high FeO (22.24 wt.%) and middle to high TiO$_2$(4.31 wt.%), is 0.18 for VNIS at Site 8 and 0.07 for M^3 data. From Figure 8(b) it cannot be determined whether the *CE-3* soil is immature or mature. It also indicates that not only the composition but also the data used for the calculation of OMAT (and other optical maturity indices) can affect the optical maturity value.

4.5 Conclusions

The *CE-3 in situ* spectra provided the unique opportunity to investigate space weathering on the lunar surface, which could not be truly investigated remotely or in the laboratory. This shows that the returned samples do not represent pristine space weathering of the lunar regolith. The upper-
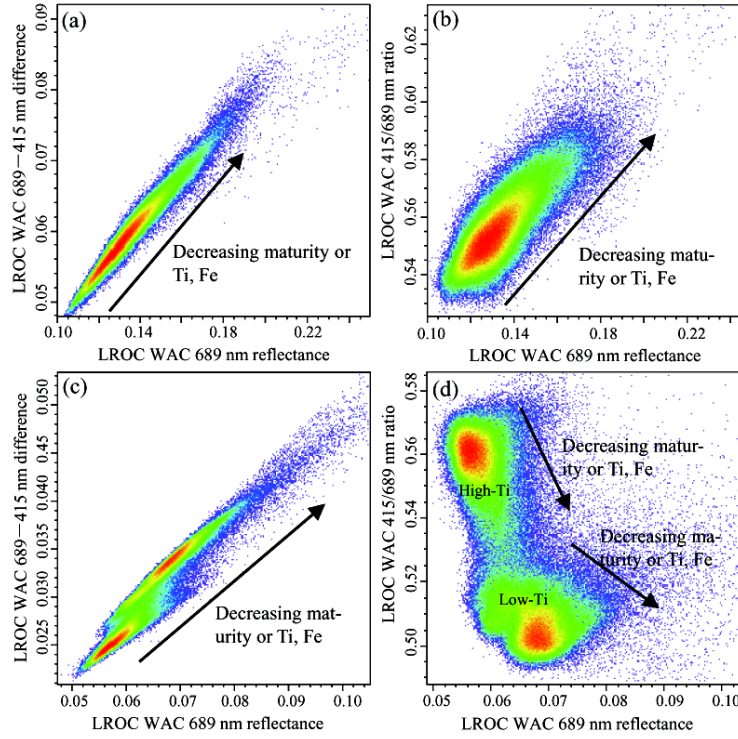
Fig. 7 Scatterplots of LROC WAC data for two areas (189 km × 189 km) from highlands and mare. (a) difference (689 nm – 415 nm) vs. reflectance (689 nm) for highlands, (b) ratio (415 nm/689 nm) vs. reflectance (689 nm) for highlands. (c) and (d) are similar to (a) and (b) but for mare.
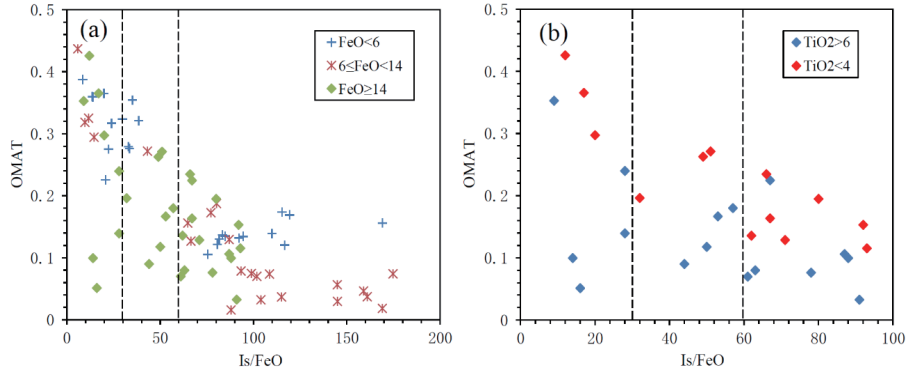

Fig. 8 (a) The OMAT versus the laboratory exposure index Is/FeO for LSCC soils. (b) The data are for samples with FeO >14 wt.%. The immature, submature and mature divisions by the two *dashed lines* are those of Morris (1976).

most surficial regolith, perhaps several millimeters to tens of centimeters thick, is much more weathered than the regolith immediately below, indicating a rapid development of SMFe and other space weathering products. The finest fraction of the skin regolith is very dark and attenuated throughout the VNIR wavelengths, indicating it is rich in various space weathering products. To study space weathering of the uppermost surface in laboratory conditions would require development of specific sampling technologies, such as electrostatically manipulating fine dust.

This study reveals that the three traditional indicators representing mature Is/FeO, VNCS and OMAT cannot accurately represent space weathering of the real surface of the Moon. All of the spectral parameters or optical maturity indices are compositionally related and hence are only valid regionally. Moreover, the optical maturity value is also related to the data source or instrument. The effects on the spectral slope caused by space weathering are wavelength-dependent: the VNCS increases while the VS decreases. At UV to VIS wavelengths, space weathering blues the regolith rather than reddens it. It has the same

sense as spectrally neutral minerals or elements (e.g., il-
menite or TiO_2). This suggests that the development of a
new TiO_2 abundance algorithm is needed. Since optical re-
mote sensing can only sense the superficial very weathered
regolith, the elements and minerals retrieved by optical
remote sensing need to be carefully evaluated. Sampling
the uppermost surface was suggested. Because the small-
est dusts are very rich in Fe^0 and easiest to be blown or
suspended, the return of these materials has implications
on investigations of the safety of an astronaut and rover,
and contributes to understanding of lunar exosphere and
material transfer, especially along the terminator.

References

Anand, M., Taylor, L. A., Nazarov, M. A., et al. 2004,
    Proceedings of the National Academy of Science, 101, 6847

Arvidson, R., Drozd, R., Guinness, E., et al. 1976, in Lunar
    and Planetary Science Conference Proceedings, 7, ed. R. B.
    Merrill, 2817

Basilevsky, A. T., Abdrakhimov, A. M., Head, J. W., et al. 2015,
    Planet. Space Sci., 117, 385

Charette, M. P., McCord, T. B., Pieters, C., & Adams, J. B. 1974,
    J. Geophys. Res., 79, 1605

Cirlin, E., Housley, R., Goldberg, I., & Paton, N. 1974, in Lunar
    and Planetary Science Conference, 5, 121

Clegg, R. N., Jolliff, B. L., Robinson, M. S., Hapke, B. W., &
    Plescia, J. B. 2014, Icarus, 227, 176

Denevi, B. W., Robinson, M. S., Boyd, A. K., et al. 2014, Journal
    of Geophysical Research (Planets), 119, 976

Drozd, R. J., Hohenberg, C. M., Morgan, C. J., Podosek, F. A.,
    & Wroge, M. L. 1977, in Lunar and Planetary Science
    Conference Proceedings, 8, ed. R. B. Merril, 3027

Fischer, E. M., & Pieters, C. M. 1994, Icarus, 111, 475

Fischer, E. M., & Pieters, C. M. 1996, J. Geophys. Res., 101,
    2225

Gillis, J. J., Jolliff, B. L., & Elphic, R. C. 2003, Journal of
    Geophysical Research (Planets), 108, 5009

Hapke, B. 2001, J. Geophys. Res., 106, 10039

Hendrix, A. R., & Vilas, F. 2006, AJ, 132, 1396

Hiroi, T., Pieters, C. M., & Morris, R. V. 1997, in Lunar and
    Planetary Inst. Technical Report, 28, Lunar and Planetary
    Science Conference, 575

Housley, R. M., Cirlin, E. H., Goldberg, I. B., et al. 1975, in
    Lunar and Planetary Science Conference Proceedings, 6, 3173

Jolliff, B. L., Wieczorek, M. A., Shearer, C. K., & Neal, C. R.
    2006, New Views of the Moon (Berlin: de Gruyter) *https:
    //www.degruyter.com/view/product/501836*

Kaydash, V., Shkuratov, Y., Korokhin, V., & Videen, G. 2011,
    Icarus, 211, 89

Keller, L. P., & McKay, D. S. 1993, Science, 261, 1305

Keller, L. P., & McKay, D. S. 1997, Geochim. Cosmochim. Acta,
    61, 2331

Keller, L. P., Berger, E. L., Christoffersen, R., & Zhang, S. 2016,
    in Lunar and Planetary Inst. Technical Report, 47, Lunar and
    Planetary Science Conference, 2525

Le Mouélic, S., Langevin, Y., Erard, S., et al. 2000,
    J. Geophys. Res., 105, 9445

Lucey, P. G., Blewett, D. T., & Hawke, B. R. 1998,
    J. Geophys. Res., 103, 3679

Lucey, P. G., Blewett, D. T., Taylor, G. J., & Hawke, B. R. 2000,
    J. Geophys. Res., 105, 20377

Lucey, P., Wieczorek, B. L., Shearer, M. A., & Nealin, C. K.
    2006, In: Jolliff, (eds.), New Views of the Moon, Rev. Mineral
    Geochem. 60, 84

Morris, R. V. 1976, in Lunar and Planetary Science Conference
    Proceedings, 7, ed. R. B. Merrill, 315

Noble, S. K., Pieters, C. M., Taylor, L. A., et al. 2001, Meteoritics
    and Planetary Science, 36, 31

Noble, S. K., Pieters, C. M., & Keller, L. P. 2007, Icarus, 192,
    629

Pearce, G. W., Strangway, D. W., & Gose, W. A. 1974, in Lunar
    and Planetary Science Conference Proceedings, 5, 2815

Pieters, C. M., Fischer, E. M., Rode, O., & Basu, A. 1993,
    J. Geophys. Res., 98, 20

Pieters, C. M., & Noble, S. K. 2016, Journal of Geophysical
    Research (Planets), 121, 1865

Shkuratov, Y., Kaydash, V., Sysolyatina, X., Razim, A., &
    Videen, G. 2013, Planet. Space Sci., 75, 28

Speyerer, E. J., Povilaitis, R. Z., Robinson, M. S., Thomas, P. C.,
    & Wagner, R. V. 2016, Nature, 538, 215

Staid, M. I., Pieters, C. M., Besse, S., et al. 2011, Journal of
    Geophysical Research (Planets), 116, E00G10

Taylor, L. A., Pieters, C. M., Keller, L. P., Morris, R. V., &
    McKay, D. S. 2001, J. Geophys. Res., 106, 27985

Wang, Z., Wu, Y., Blewett, D. T., et al. 2017, Geophys. Res. Lett.,
    44, 3485

Wu, Y., Besse, S., Li, J.-Y., et al. 2013, Icarus, 222, 283

Wu, Y., & Hapke, B. 2018, Earth and Planetary Science Letters,
    484, 145

Wu, Y., Li, L., Luo, X., et al. 2018a, Icarus, 303, 67

Wu, Y., Wang, Z., Cai, W., & Lu, Y. 2018b, AJ, 155, 213